

Prediction of Effective Thermal Conductivity of Refractory Materials at High Temperatures based on Synthetic Geometry Generation

C. Demuth^{*1}, J. Hubálková², M.A.A. Mendes^{1, 3}, F. Ballani⁴, D. Trimis^{1, 3}, S. Ray¹

¹Institute of Thermal Engineering, Technische Universität Bergakademie Freiberg,
Gustav-Zeuner-Straße 7, D-09596 Freiberg, Germany

²Institute of Ceramic, Glass and Construction Materials, Technische Universität
Bergakademie Freiberg, Agricolastraße 17, D-09596 Freiberg, Germany

³Engler-Bunte-Institute, Division of Combustion Technology, Karlsruhe Institute
of Technology, Engler-Bunte-Ring 7, D-76131 Karlsruhe, Germany

⁴Institute of Stochastics, Technische Universität Bergakademie Freiberg,
Prüferstraße 9, D-09596 Freiberg, Germany

received January 11, 2016; received in revised form March 21, 2016; accepted April 13, 2016

Abstract

In the present article, the numerical prediction of the effective thermal conductivity (k_{eff}) of low-carbon refractory materials at high temperatures is investigated. The employed numerical methodology consists of computational geometry generation by a modified random sequential adsorption (RSA) algorithm and solution of a heat conduction problem in the generated material sample by the finite volume method (FVM). The probability distributions, employed for modelling the grain sizes, are reexamined. Several aspects are recognised as crucial for reasonable predictions of k_{eff} in the considered range from the room to the coking temperature. First, an appropriate estimate of the equivalent thermal conductivity k_{rest} of the unresolved fine-scaled material is required, which is obtained from the effective medium theory (EMT). Furthermore, modelling the thermal expansion of the coarse and medium grains, leading to the formation of air gaps between the grains and the continuous phase at lower temperature, is extremely important. The presence of these air gaps could be implemented in FVM. The numerical predictions of k_{eff} show reasonably good agreement with experimental data in the complete temperature range, only if this gap width is considered as a function of the operating temperature, along with k_{rest} and the temperature-dependent thermal conductivities of the constituents.

Keywords: Effective thermal conductivity, refractory materials, random sequential adsorption, finite volume method, thermal contact resistance

I. Introduction

Carbon-bonded alumina refractories are widely employed in continuous steel casting processes^{1–3} as functional components, e.g. nozzles, submerged entry nozzles and ladle shrouds^{1, 2, 4}. In order to reduce CO₂ emissions from the process as well as contamination of the steel melt by carbon pickup⁵ with regard to clean steel technology⁶, ongoing research aims to reduce the carbon content in carbon-bonded alumina refractories as far as possible. Nevertheless, refractories employed in steel plants have to meet several crucial requirements, e.g. high corrosion and erosion resistance, low wettability by steel melt and slag, high mechanical strength, thermal shock and oxidation resistance at elevated temperatures^{1, 3}. In particular, the materials' thermophysical properties are of interest in order to ensure the required insulation capability and resistance to thermomechanical failure. Behaviour of the material under thermal load can be characterised by the effective thermal conductivity k_{eff} . Besides the experimental determination

of k_{eff} of the prepared material samples, their numerical prediction is also considered a valuable means that assists the material development process. In this regard, the geometrical modelling of refractory materials is essential for a deeper understanding of the influence of material structure on k_{eff} , particularly because experimental techniques (such as computed tomography scan images) for obtaining the detailed three-dimensional morphology of the material are not well established.

The methodology of predicting k_{eff} of complex composite materials was presented earlier by Zehmisch *et al.*^{7, 8}, which consists of two essential steps: the geometrical modelling of the material's structure and the subsequent numerical solution of the heat conduction problem⁹. Therefore, a synthetic geometry is first created by employing a stochastic geometry generation algorithm, while considering different material parameters known from the experimental preparation of present carbon-bonded alumina refractories. The mass fractions of the individual constituents, according to the material's composition, are converted into the corresponding volume fractions using

^{*} Corresponding author: cornelius.demuth@iwtt.tu-freiberg.de

the densities of the raw materials and the measured value of overall porosity⁸. The grain size distributions of the constituents were measured by means of laser diffraction analysis and are modelled using either the lognormal distribution or the Rosin-Rammler-Sperling-Bennett^{10–12} (RRSB) distribution. In addition, the grain shapes of different components were observed from the scanning electron microscopy (SEM) images and are approximated by basic polyhedral shapes during the geometry generation process. The discrete phase distribution is created in the computational domain, which is then subjected to a temperature difference by keeping two walls facing each other at constant as well as uniform hot and cold temperatures, while the remaining walls are considered to be adiabatic. The heat conduction equation is solved in this domain by suitable numerical techniques, e.g. Finite Volume Method (FVM)^{13,14} or Thermal Lattice Boltzmann Method (TLBM)⁹. Based on the steady-state solution of the heat conduction problem, k_{eff} is numerically evaluated according to the averaged Fourier's law. This methodology for predicting k_{eff} of composite material is similar in principle to the one applied for porous foams¹⁵.

A sensitivity analysis of k_{eff} determined at room temperature on several parameters of the model, e.g. direction of the applied temperature gradient, randomness in the generated geometry, shape of grains and equivalent thermal conductivity of the unresolved material, was also performed in the earlier work⁸. However, recent experimental data reveal distinctly lower k_{eff} of the modelled refractory material as compared to those reported earlier^{7,8}. For this reason, several aspects of the numerical methodology are revisited in the present investigation, e.g. the approximation of constituents' grain size distributions and the modelled thermal conductivity of the unresolved fine-scaled material. In addition, the prediction of k_{eff} of the refractory material at high temperatures was not covered in previous study^{7,8} and is hence one of the major objectives of the present investigation. Preliminary numerical results showed that, using the described methodology^{7,8}, the predicted k_{eff} at elevated temperatures up to 1200 °C significantly underestimated the experimentally observed trend.

In the present article, the issues related to excessive reduction in the numerically determined k_{eff} of the considered refractory material at higher temperatures, as compared to k_{eff} predicted at the room temperature, are investigated. For this purpose, not only the temperature-dependent thermal conductivities of the components are considered, but also the thermal expansion mismatch between coarse or medium grains with regard to the continuous phase, when these are cooling down from the coking to the room temperature, are taken into account. By the latter, gaps are introduced adjacent to the coarse and medium grains constituting porosity^{16,17}. As an additional contribution to k_{eff} at higher temperatures, the effect of thermal radiation¹⁸ is also investigated. This effect is considered since it is also found to be relevant for porous foams^{19,20}. In this regard, the contribution of radiative heat transfer can be considered through the Rosseland approximation¹⁸ if the optical thickness of the porous medium is relatively high, which is the case for porous media with relatively small pores like the one considered for the present study.

The present article consists of five sections. This short introduction is followed by the experimental investigation, providing details on the production and the experimentally determined properties of the considered refractory material. The numerical methodology, dealing with both stochastic geometry generation and solution of heat conduction problem in the modelled domain, is outlined in section III, while section IV presents and discusses the results of predicted k_{eff} at higher temperatures. Finally, conclusions from the present study are drawn and an outlook on the prospective work is presented in section V.

II. Experimental Investigation

Al₂O₃-C refractory materials, with reduced carbon content, were developed at the Institute of Ceramic, Glass and Construction Materials of Technische Universität Bergakademie Freiberg, Germany. A reference for the investigation of such materials is the refractory composition with a primary carbon content of 20 wt% as shown in Table 1, where the antioxidant fine metallic silicon powder in the basic composition R20^{1,21} was replaced by the fraction of fine tabular alumina. For coarse refractories, the raw material grades are divided into coarse fractions with grain sizes greater than 1 mm, medium grains from 0.1 mm to 1 mm and fine grain fractions smaller than 0.1 mm^{22,23}. However, since the largest grain sizes in the considered composition R20 are in the submillimetre range, the fractions of tabular alumina (0.2–0.6 mm) and coarse graphite represent the coarse grains, while the medium grains are considered to be those of fused alumina (0–0.2 mm).

The motivation for employing a wide distribution of grain sizes or a mixture of different grain sizes in the composition is to obtain improved particle packing and higher density of the composite that occur due to the enhanced densification during production²⁴. In this manner, the finer particles are allowed to fit into the interstices of the coarser grains²⁵. In particular, the compaction of a composition during uniaxial pressing is facilitated for a wider particle size distribution²⁴.

Tabular and fused alumina, liquid resin (novolac), coarse and fine graphite were first mixed in an Eirich intensive mixer at room temperature with a final addition of the binder in powder form and the curing agent hexamethylenetetramine. The mixture was then uniaxially pressed to the size of standard bricks at 100 MPa. Subsequently, the pressed samples were cured at 180 °C for two hours. In the curing process, the resin is polymerised under addition of the curing agent and a three-dimensional, cross-linked, resite lattice is formed²⁶.

Finally, the samples were coked for five hours in a furnace at 1000 °C under reducing conditions, i.e. embedded in a retort filled with coke. The coking process comprises a pyrolysis, i.e. the resite lattice transforms into elementary carbon, constituting an amorphous carbon lattice. As several other complex reactions, e.g. condensation, dehydrogenation and isomerisation, take place along with pyrolysis²⁶, the coking process is conceived as a carbonisation. The residual carbon content, i.e. the carbon mass fraction remaining after carbonisation as compared to the mass of phenolic resin binder (novolac) with hexamethylenetetramine²⁶, was reported to be in the range from 45–50 %^{26,27} up to 60 %²⁸.

The bulk density and the open porosity of the coked samples were determined according to the standard DIN EN 993 – 1 using the toluene displacement method. The true density of the samples was measured using a pycnometer in accordance with the standard DIN EN 993 – 2. Subsequently, their overall porosity was determined using the bulk and the true densities, cf. DIN EN 993 – 1. The measurement of thermal conductivity of carbon-containing refractory materials by the hot-wire method at temperatures up to 800 °C was presented earlier by Tomczek and Suwak²⁹.

In the present work, the thermal conductivity of the coked samples of dimensions 223 mm × 122 mm × 68 mm was measured in the range from room temperature up to 1000 °C using the parallel hot-wire technique according to the standards ISO 8894 – 2 and DIN EN 993 – 15 as far as practicable. As a deviation from the standards, the samples were embedded in coke inside a corundum box in order to avoid oxidation of carbon from the samples at elevated temperatures. Furthermore, K-type thermocouples, instead of the standard R- or S-type thermocouples, were employed as measuring and reference thermocou-

ples, since platinum reacts with carbon at higher temperatures. For the same reason, the hot wire was protected by a corundum capillary tube. In addition, the reference thermocouple was placed beside the sample inside the corundum box.

The microstructure of material samples was investigated by scanning electron microscopy (SEM) using either the secondary electron or the backscattered electron detector. SEM micrographs of the material structure with two different magnifications are presented in Fig. 1. The alumina grains can be easily recognised in the contrast images in Figs. 1(c) and (d) by their brightness as compared to the darker graphite and amorphous carbon fractions.

The volume fractions of different phases were then determined according to the procedure suggested earlier⁸, taking different aspects into account: the mass fractions and the densities of raw materials, the residual carbon content of the binder and the porosity of the continuous phase that is reported in Table 1. The resulting volume fractions, employed for the geometry generation, are also reported in Table 1.

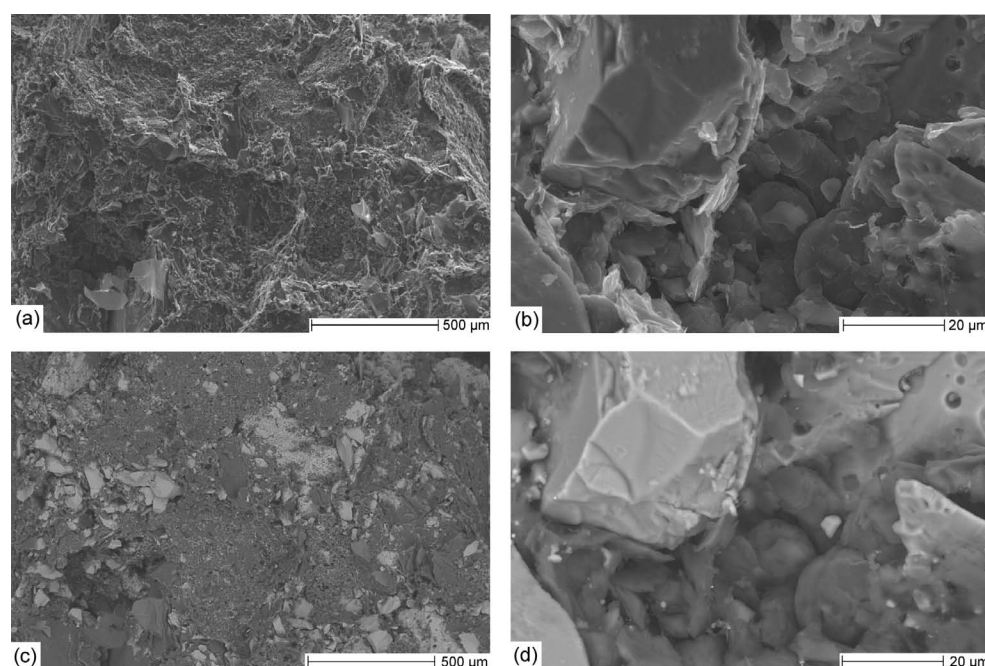


Fig. 1: Scanning electron micrographs of the material structure of R20 samples: detail of approximately (a), (c) 1.9 mm × 1.2 mm and (b), (d) 95 μm × 60 μm.

Table 1: Mass and volume fractions of reference refractory composition R20.

Raw material	w_n [wt%]	ϱ [g/(cm) ³]	ϱ_{ref} [g/(cm) ³]	ϕ_n [%]
Coarse tabular Al ₂ O ₃	38.9	3.95–4.1	4.0	25.0
Fused Al ₂ O ₃	29.1	3.95–4.1	4.0	18.7
Fine tabular Al ₂ O ₃	6.0	3.95–4.1	4.0	3.8
Coarse graphite	10.0	1.9–2.3	2.0	12.8
Fine graphite	10.0	1.9–2.3	2.0	39.7
Novolac liquid	} Glass-like C	2.0	1.8	
Novolac powder		4.0		
Hexamethylenetetramine	0.6	thereof porosity p		23.0

Considering the aforementioned parameters from the previous investigation⁸, it may be recognised that the most prominent error in the determination of volume fractions arises from the uncertainty in the density of graphite and the residual carbon content. For a density of graphite lower than the reference value, the volume fractions of graphite could be 3.5 % higher and those of the other constituents, particularly alumina, could be 1.7 % lower relative to the volume fractions shown in Table 1. In case of a higher density of graphite, the volume fractions of graphite could be 9 % lower and that of the other constituents could be 4.5 % higher. In the latter situation, the volume fraction of the unresolved fine-scaled material would be 2.5 % lower relative to the value stated in Table 1. Similarly, a higher residual carbon content of 60 % instead of 45 % would increase the volume fraction of amorphous carbon by at least 30 % and, consequently, that of the unresolved fine-scaled material would increase by 2.4 %.

It may be recognised that part of the porosity is formed due to the thermal expansion mismatch between the coarse/medium grains and the amorphous carbon lattice. The thermal expansion of raw materials occurs to a much greater extent during the coking process as compared to thermal expansion of the binder. While cooling down, however, raw grains shrink distinctly, but the carbon lattice, resulting from pyrolysis of the binder materials, does not shrink to that extent owing to the significantly lower coefficient of thermal expansion of the glass-like carbon as compared to graphite and alumina¹⁷, as may be observed from Table 2. Therefore, voids are generated adjacent to the glass-like carbon lattice. This part of the overall porosity is accommodated in the numerical model using the temperature-dependent gap width, separating the continuous phase from the coarse and the medium grains. Therefore, the contact between the grains of raw materials and the carbon lattice increases due to thermal expansion when the material is heated to higher temperatures.

The volumetric grain size distributions of fused alumina, tabular alumina, coarse graphite and fine tabular alumina were measured using the laser diffraction particle size analysis. The probability distributions, considered for the description of particle size distributions, are the lognormal and the Rosin-Rammler-Sperling-Bennett (RRSB) distribution^{10–12}, the latter also being known as the Weibull distribution³⁰.

III. Numerical Methodology

(1) Geometry generation

Along with the volume fractions, determined according to the calculation presented in the earlier study⁸, the grain size distributions of the raw materials are required to be approximated in order to realise a representative model of the refractory material. For this purpose, the grain diameters d_i are expressed in terms of $b_i = \ln(d_i/d_{\text{ref}})$, where $d_{\text{ref}} = 1$ mm is employed in the present investigation. The size range of 0.04 μm –2 mm, covered during experiments, is divided in-

to 116 bins with $\Delta b = 0.093$. The volume fractions p_i in the i^{th} bin are divided by the bin width according to^{31–33}

$$q_{3,i} = \frac{p_i}{\Delta b_i}, \quad (1)$$

where the subscript 3 indicates a volume distribution, to obtain a histogram, compatible with the depiction of a theoretical particle size density distribution. The cumulative grain size distribution function is known at the interval bounds $d_i = d_{\text{ref}}e^{b_i}$ and is given by:

$$Q_{3,i} = Q_3(e^{b_i}) = F_V(e^{b_i}) = \sum_{j=1}^i p_j. \quad (2)$$

The lognormal distribution is characterised by the cumulative distribution function

$$Q_3(e^b) = F_V(e^b) = \frac{1}{\sigma\sqrt{2\pi}} \int_{-\infty}^b \exp\left[-\frac{(b' - \mu)^2}{2\sigma^2}\right] db'. \quad (3)$$

The location parameter μ (the logarithm of the median grain diameter) and the scale parameter σ (the standard deviation of the logarithmised grain diameter b) are determined according to the standard DIN 66144 as:

$$\mu = \ln\left(\frac{d_{50}}{d_{\text{ref}}}\right), \sigma = \ln\left(\frac{d_{50}}{d_{16}}\right) \text{ or } \sigma = \ln\left(\frac{d_{84}}{d_{50}}\right). \quad (4)$$

On the other hand, the cumulative distribution function of the two-parameter RRSB distribution is given by: 10–12, 30

$$Q_3(e^b) = F_V(e^b) = 1 - \exp\left[-\left(\frac{e^b}{\lambda}\right)^n\right], n, \lambda > 0 \quad (5)$$

with shape n and scale λ as parameters, which are obtained by employing the transformation^{31, 33}

$$\ln(-\ln(1 - F_V(e^b))) = nb - n \ln \lambda \quad (6)$$

from the slope and the intercept of the resulting linear function, respectively, according to the standard DIN 66145.

Considering the measured grain size distributions, it is found that the grain size distributions of different alumina grades can be approximated by the lognormal distributions. On the other hand, the grain size distribution of coarse graphite more closely resembles an RRSB probability density function. This may be observed from Fig. 2, where the approximated probability density functions are presented along with $q_{3,i}$ according to Eq. (1), for tabular alumina and coarse graphite. The determined probability distribution parameters are provided in Table 3 for different raw materials.

Random grain sizes, distributed according to a lognormal law, are generated using the algorithm for normal deviates^{34, 35} of logarithmised grain size and subsequent exponentiation³⁶. Furthermore, the fundamental transformation law of probabilities^{35, 37} is employed in order to generate random grain sizes obeying the RRSB distribution by the inverse of Eq. (5) given by³⁵

$$x = \lambda[-\ln(1-y)]^{1/n}, y \in (0,1) \quad (7)$$

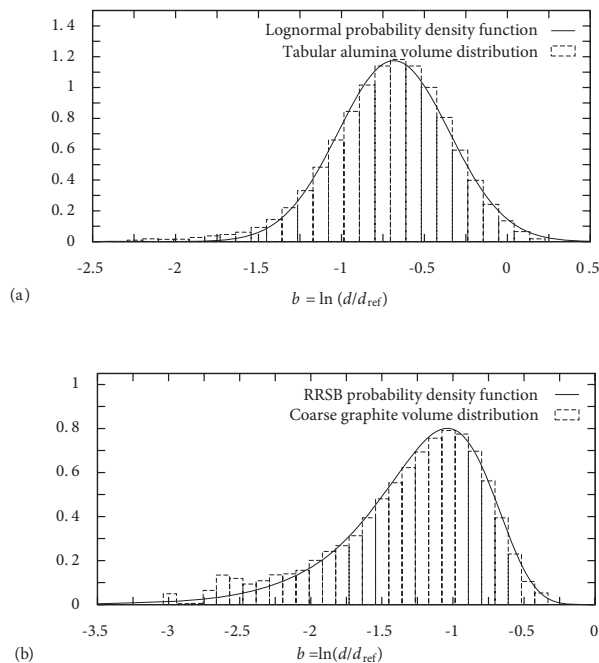
Table 2: Linear thermal expansion coefficients of constituents at different temperatures ^{48–51}.

Temperature [°C]	20	100	200	300	400	500	600	700	800	900	1000
Constituents	Linear thermal expansion coefficient α [10^{-6} 1/K]										
Tabular alumina	5.4	7.1	7.4	7.8	8.1	8.5	8.8	9.1	9.3	9.6	9.8
Fused alumina	7.6	7.8	8.0	8.2	8.4	8.6	8.9	9.1	9.3	9.5	9.7
Graphite ()	-1.25	-1.0	-0.65	-0.25	0.05	0.28	0.5	0.65	0.8	0.91	0.97
Graphite (\perp)	25.0	27.5	28.0	28.0	28.0	28.3	28.5	28.9	29.5	30.5	31.2
Graphite (av.)	7.5	8.5	8.9	9.2	9.4	9.6	9.8	10.1	10.4	10.8	11.0
Glass-like carbon	3.1	3.2	3.3	3.3	3.4	3.5	3.6	3.8	3.9	4.0	4.2

Table 3: Parameters of approximated grain size distribution functions for different raw materials.

Lognormal distr. param.	Coarse tab. Al_2O_3	Fused Al_2O_3	Fine tab. Al_2O_3	RRSB distr. parameters	Coarse graphite
Location μ	-0.684	-2.684	-2.996	Scale λ	0.354
Scale σ	0.335	0.72	0.50	Shape n	2.576

from random uniform deviates y in the unit interval. It should also be noted here that the approximated grain size distributions describe a volume instead of a count distribution. For this reason, a reference volume is related to the volume of a grain of each random diameter for the determination of number of grains of this particular size to be inserted during the geometry generation.

**Fig. 2:** Measured grain size distributions of raw materials and their approximations: (a) lognormal distribution for coarse tabular Al_2O_3 and (b) RRSB distribution for coarse graphite.

The polyhedral grain shapes, assumed according to the SEM images, are truncated pentagonal prisms for different alumina grades and hexagonal prisms for coarse graphite platelets. In addition, since grain shapes are not rotationally symmetric, random Euler angles are generated for each

grain and the grain is rotated according to the “x-y-z convention” ³⁸ before its placement into the generated geometry.

The modified RSA algorithm, employed due to a high overall volume fraction of the packing, has already been presented earlier ^{7,8}. According to this algorithm, grains of random size are added sequentially and randomly into the computational domain ³⁹, starting with the coarsest component. Both position and angles of rotation of each grain to be placed are randomly generated. The modification of RSA algorithm consists in allowing grains of the same constituent to overlap, whereas the grains corresponding to different raw materials are not allowed to overlap. Whenever the placement of a particular grain is rejected, it is reattempted at a different random position retaining the angle of rotation. Once the prescribed volume fraction of a component is reached, the algorithm continues with the insertion of the grains of the next component until the grains of all components are placed.

The phase distribution of a generated geometry consisting of 200^3 voxels representing the $(2 \text{ mm})^3$ sample of the refractory material R20 with a resolution of $10 \mu\text{m}$ is shown in Fig. 3. The thermal conductivities of the individual phases are prescribed for solving the heat conduction problem. As observed in the previous study ⁸, the predicted k_{eff} is sensitive towards the equivalent thermal conductivity k_{rest} of the unresolved material. However, it is observed during the present investigation that the previously ^{7,8} employed upper Hashin-Shtrikman ⁴⁰ bound for k_{rest} results in considerable overprediction of k_{eff} as compared to the experimental data. Consequently, the effective medium theory ⁴¹ (EMT) is adopted in order to estimate k_{rest} .

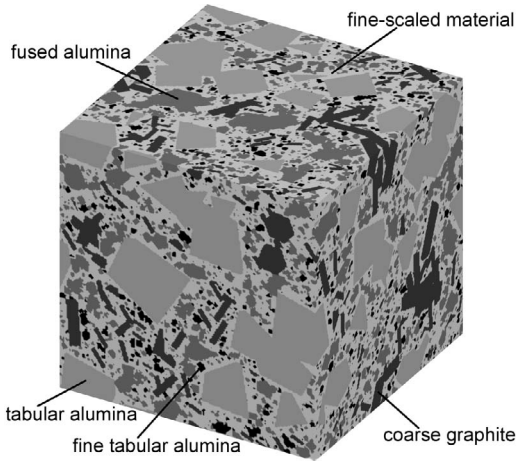


Fig. 3: Generated phase distribution representing cube of 2 mm side of the modelled refractory material R20 employing 200^3 voxels.

The effective thermal conductivity of the three components, namely fine graphite denoted by the subscript 1, amorphous carbon marked as phase 2 and porosity labelled as phase 3, present in the unresolved phase, is determined according to EMT in a two-step procedure⁴². First, the effective thermal conductivity $k_{\text{eff},12}$ of the two components fine graphite and amorphous carbon is determined by

$$k_{\text{eff},12} = \frac{1}{4} \left\{ f(k_1, k_2) + \sqrt{f^2(k_1, k_2) + 8k_1k_2} \right\}, \quad (8)$$

$$f(k_1, k_2) = \left(3 \frac{\phi_1}{1 - \phi_3} - 1 \right) k_1 + \left(3 \frac{\phi_2}{1 - \phi_3} - 1 \right) k_2,$$

where the volume fractions ϕ_n of the three phases are considered relative to that of the unresolved material ϕ_{rest} as part of the composition. In Eq. (8), the volume fractions ϕ_1, ϕ_2 are related to their sum, which represents the complement of the porosity (volume fraction ϕ_3) in the unresolved material. In the second step, $k_{\text{eff},12}$ obtained from Eq. (8) is employed in the analogous determination

$$k_{\text{rest}} = \frac{1}{4} \left\{ f(k_{\text{eff},12}, k_3) + \sqrt{f^2(k_{\text{eff},12}, k_3) + 8k_{\text{eff},12}k_3} \right\}, \quad (9)$$

$$f(k_{\text{eff},12}, k_3) = (3(\phi_1 + \phi_2) - 1)k_{\text{eff},12} + (3\phi_3 - 1)k_3.$$

(2) Determination of k_{eff}

After generating the random geometry, k_{eff} of the modelled material is obtained by applying the averaged Fourier's law

$$k_{\text{eff}} = \frac{L}{T_h - T_c} \dot{q}_{\text{av}}'' = \frac{L}{T_h - T_c} \frac{\int_A \dot{q}'' dA}{\int_A dA} \quad (10)$$

using the averaged steady-state heat flux \dot{q}_{av}'' obtained from a heat conduction problem, where a temperature difference $T_h - T_c$ is applied across a length L between two opposite faces of the computational domain and the remaining faces are considered to be adiabatic. In the present article, the finite volume method (FVM) is employed in order to solve the integral form of steady-state heat conduction equation without heat source in the composite medium:

$$\int_V \nabla \cdot (k \nabla T) dV = 0 \quad (11)$$

where the thermal conductivity varies spatially, i.e. $k = k(x)$.

The computational domain is discretised using a finite number of control volumes with their faces defined by an equidistant Cartesian grid, where the nodes are located at the centres of each control volume. In addition, nodes are also arranged at the faces, edges and corners of the computational domain for the easy implementation of boundary conditions. The phase information, resulting from the geometry generation, is associated with each control volume. The steady-state heat conduction equation (11) is rewritten in its discrete form employing a second order accurate central differencing scheme for the spatial derivatives.

In detail, the second order spatial derivatives in Eq. (11) are computed as a difference quotient of the product of thermal conductivity and first derivative using central difference approximation, i.e. both being evaluated at the cell faces of the succeeding and preceding control volumes in the respective coordinate direction. Without the loss of generality, let i be the index of the current control volume with respect to the coordinate direction x as well as $i + 1$ and $i - 1$ those of its successor and predecessor, respectively. In the present case of an equidistant Cartesian grid, the faces of cell i adjacent to its neighbours are situated exactly halfway between the cell centres and hence may be denoted by $i + 1/2$ and $i - 1/2$. The cell face conductivities employed in the second derivative approximation are evaluated by the harmonic mean

$$k_{i \pm 1/2}^\perp = \left(\frac{1}{2k_i} + \frac{1}{2k_{i \pm 1}} \right)^{-1} \quad (12)$$

corresponding to the series arrangement of the adjacent control volumes' phases. In particular, Eq. (12) results in $k_{i \pm 1/2}^\perp = k_i$ for $k_i = k_{i \pm 1}$. It should be noted here that the thermal conductivity, associated with the phase attributed to an arbitrary control volume, only enters the computation on the right hand side of Eq. (12).

The resultant linear system of equations is solved implicitly using the method of conjugate gradients⁴³. From the computed steady-state temperature distribution, the heat fluxes required for the evaluation of k_{eff} in Eq. (10) are obtained as a function of the temperature gradient at the relevant boundaries. It should also be noted that the referred FVM is implemented in an in-house code which has been suitably parallelised and thoroughly verified by solving several benchmark problems^{7,44}.

In order to determine k_{eff} at different temperatures, the thermal conductivities of different components, employed in the heat conduction solver, are specified as functions of their temperature that mostly decrease with the increase in temperature. The thermal conductivity data of all constituents at different temperatures are provided in Table 4. Nevertheless, k_{eff} predicted in this manner are found to notably overestimate the experimental data, particularly at low and moderate temperatures, as shall be presented later in this article. It appears obvious that the lower experimental observations may be attributed to the thermal expansion mismatch between the grains of raw materials and the amorphous carbon lattice which

produces thin intermediate air gaps after coking at high temperature and subsequent cooling down to the room temperature. The thickness of the air gap reduces with the increase in temperature and vanishes as the temperature of the medium is again raised to the original coking temperature. Since the gap width is extremely small (in the range from submicron to few microns) to be resolved by the numerical grid, the reduced thermal contact between either coarse or medium grains and the continuous phase is accounted for in the FVM code by considering a modified series arrangement of the two adjacent phases with an intermediate air layer of width l_c as depicted in Fig. 4. In this context, the subscript c indicates the reduced thermal conductivity due to the air gap. The equivalent thermal conductivity between two adjacent nodes for such a configuration is given by

$$k_c^\perp = \left(\frac{1-l_c^*}{2k_n} + \frac{l_c^*}{k_{\text{air}}} + \frac{1-l_c^*}{2k_{\text{rest}}} \right)^{-1}, \quad (13)$$

where the subscript n denotes the phase of the coarse or medium grain and the gap width l_c^* is normalised in respect of the grid spacing. The thermal conductivity for the modified series arrangement in Eq. (13) is considered in the respective coefficients in the FVM code wherever the respective phases, i.e. the coarse or the medium grain and the continuous phase, are in direct contact. Otherwise, the conventional series arrangement of the two phases analogous to Eq. (12), obtained with $l_c^* = 0$ in Eq. (13), is employed.

IV. Results and Discussion

In the present investigation, k_{eff} of the considered refractory material is determined numerically at temperatures 20 °C, 100 °C, 200 °C up to 1000 °C at intervals of 100 K. For this purpose, the thermal conductivities and the coefficients of thermal expansion of the constituents are required as functions of temperature. The thermal conductivities at different temperatures ranging from 20 °C to 1000 °C can be found in the literature for alumina⁴⁵, graphite⁴⁶, amorphous carbon (glass-like carbon)⁴⁶ as well as for air⁴⁷ that is present in the pores and the thin gap between the resolved grains and the continuous phase. These values, adopted for individu-

al components at different temperatures, are provided in Table 4. It should be noted that since graphite exhibits an anisotropic behaviour for its thermal conductivity, the geometric mean of the thermal conductivities in the directions parallel and perpendicular to the crystal structure, i.e. $k = (k^\parallel k^\perp)^{1/2}$ is employed for the numerical predictions. The thermal conductivities of the constituents, except glass-like carbon and air, significantly decrease with the increase in temperature as may be observed from Table 4, which also shows that the typical thermal conductivities at 1000 °C are approximately one third of those at the room temperature.

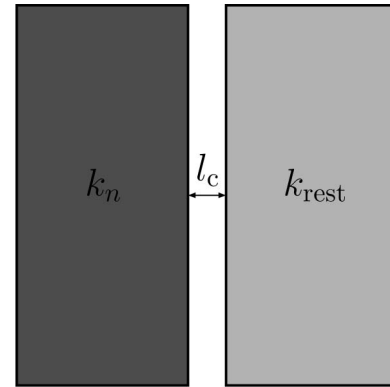


Fig. 4: Modified series arrangement with air gap of width l_c between coarse or medium grain and continuous phase.

The experimental data for k_{eff} , however, do not exhibit such a distinct decrease at higher temperatures, as may be observed from Fig. 5. As a remedy, the thermal expansion of the grains is taken into account in order to enable reasonable numerical predictions at higher temperatures. The linear thermal expansion coefficients in the considered temperature range are available from the literature for alumina⁴⁸, corundum (fused alumina)⁴⁹, graphite^{50,51} and glass-like carbon⁴⁸, that are already presented in Table 2. As expected, the graphite grains show strong anisotropy with more pronounced variation of the thermal expansion coefficient perpendicular to the crystal structure. Therefore, the linear thermal expansion coefficient of graphite is modelled as: $\alpha = 2\alpha^\parallel/3 + \alpha^\perp/3$.

Table 4: Thermal conductivities of constituents at different temperatures^{45–47}.

Temperature [°C]	20	100	200	300	400	500	600	700	800	900	1000
Thermal conductivity k [W/(mK)]											
Alumina	31.8	28.2	24.1	21.4	18.9	17.1	15.6	14.6	13.4	12.3	11.4
Graphite (\parallel)	165	150	131	116	102	90.6	80.3	71.7	64.4	57.6	51.6
Graphite (\perp)	119	111	96.3	84.6	75.1	67.4	60.7	54.4	48.8	43.6	38.9
Graphite ($(k^\parallel k^\perp)^{1/2}$)	140	129	112	99.1	87.5	78.1	69.8	62.5	56.1	50.1	44.8
Glass-like carbon	1.59	1.82	2.02	2.16	2.26	2.35	2.42	2.50	2.62	2.79	2.97
Air [mW/(mK)]	25.9	31.6	38.2	44.4	50.2	55.8	61.1	66.3	71.3	76.3	81.1

It may be recognised from Table 2 that the linear thermal expansion coefficients of alumina and graphite are of the order of 10^{-5} 1/K. For the numerical determination of k_{eff} , however, the following simplifications are assumed. The aforementioned order of magnitudes for α and a temperature difference of approximately 1000 K result in the corresponding thermal expansions of 5 μm and 1 μm for coarse (≈ 0.5 mm) and medium (≈ 0.1 mm)-sized grains. Consequently, the air gaps between either coarse or medium grains and the continuous phase are assumed to be either 1/2 or 1/10 of the presently used grid size of 10 μm , i.e. $l_c^* = 1/2$ or $l_c^* = 1/10$, respectively, at room temperature. At elevated temperatures, however, the thermal expansion of the coarse- and medium-sized grains results in a decrease in the associated normalised air gaps l_c^* that are assumed to vary linearly from their room temperature values to zero at the coking temperature of 1000 °C.

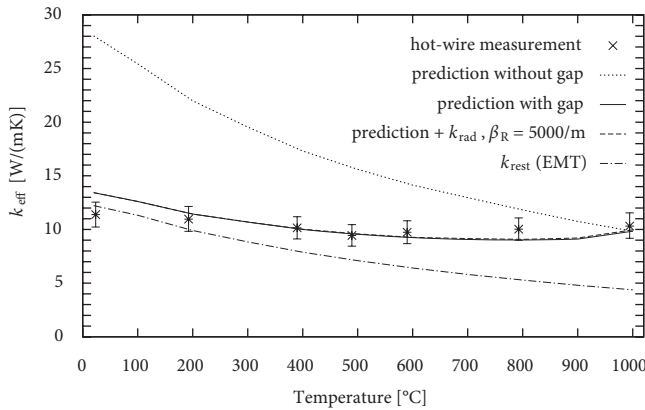


Fig. 5: Measured and predicted k_{eff} at different temperatures.

Employing the temperature-dependent thermal conductivities of the components, mentioned in Table 4, and k_{rest} determined by EMT in Eqs. (8) and (9), k_{eff} of the modelled carbon-bonded refractory composition is numerically predicted. The results, presented in Fig. 5, clearly show that k_{eff} is significantly overestimated at room and moderate temperatures as compared to the experimental data obtained by the parallel hot-wire method, if the gap between the coarse/medium grains and the continuous phase is not taken into account. The modelled k_{rest} as a function of temperature is also presented in Fig. 5 for the sake of clarification. Therefore, the air gap between the coarse/medium grains and the continuous phase, which decreases with the increase in temperature, is considered according to the aforementioned assumptions, which markedly improves the predictions of k_{eff} in the considered temperature range, as may be observed from Fig. 5. It is evident that although an overprediction of k_{eff} is obtained at the room temperature, the numerical predictions closely follow the experimental trend over the entire temperature range.

The predictions of k_{eff} are obtained by the in-house FVM code, using its parallel processing features. The steady-state heat conduction equation (11) is solved in its dimensionless form, where the non-dimensional temperature is defined as $\theta = (T - T_c)/(T_h - T_c)$. The iterative solution of the resultant linear system of discretised equations is accepted once the change in the iterate satisfies the following convergence criterion ⁴⁴

$$\frac{\sqrt{\sum_{i,j,k} (\theta_{i,j,k}^{\text{new}} - \theta_{i,j,k}^{\text{old}})^2}}{n_i n_j n_k} < \varepsilon = 10^{-12}, \quad (14)$$

where i, j, k denote the indices of the nodes in the x, y, z directions and n_i, n_j, n_k are the numbers of nodes in the respective direction. Employing eight cores on an available high performance compute cluster, convergence according to Eq. (14) is achieved after approximately 2300–3600 iterations for the predictions of k_{eff} consuming about 800 s – 1200 s of computational time. The number of iterations as well as the required computational time are observed to increase with the employed width of the air gap.

In addition, the numerical predictions at higher temperatures may be augmented by the contribution of thermal radiation to k_{eff} according to:

$$k_{\text{eff}} = k_{\text{cond}} + k_{\text{rad}} \quad (15)$$

with the radiative term resulting from the Rosseland approximation: ¹⁸

$$k_{\text{rad}} = \frac{16n^2\sigma T^3}{3\beta_R}, \quad (16)$$

where n is the refractive index, $\sigma = 5.67 \times 10^{-8}$ W/(m²K⁴) is the Stefan-Boltzmann constant and β_R is the Rosseland-mean extinction coefficient.

The extinction coefficient β may be estimated from the transmittance τ of a considered sample thickness l according to $\beta = -\ln(\tau)/l$ employing the Beer-Lambert law ⁵². Considering paths along each of the coordinate directions in the generated geometry, a path consisting of only voxels representing the unresolved fine-scaled material comprising the porosity is hardly found. Consequently, the transmittance is expected to be at most 1/40000 and hence the extinction coefficient is bounded from below by the value 5000 1/m for a sample thickness of 2 mm. A similar lower bound for β may be found from the volume scattering theory for packed beds of opaque spheres ⁵³ assuming spherical coarse and medium grains of uniform size. Thermal radiation is conceived as electromagnetic radiation in the wavelength ranging from 100 nm to 100 μm ¹⁸. Concerning the refractive index n of the refractory material, different alumina and graphite grains are treated as opaque and thermal radiation is supposed to propagate only through the continuous phase. Consequently, a refractive index of unity representing air in the pores is considered, despite largely higher values of n for alumina and graphite in the considered range of wavelengths ⁵⁴.

Employing the aforementioned refractive index of unity and an extinction coefficient of 5000 1/m, there is only a minor enhancement of k_{eff} according to Eqs. (15) and (16). The prediction is hardly distinguishable from the one without the radiative contribution, as may be observed from Fig. 5.

V. Conclusions

The present article deals with the numerical prediction of k_{eff} of novel low-carbon refractory materials at high temperatures. For this purpose, several aspects of the numerical methodology, presented earlier ^{7,8}, are revisited.

For the stochastic geometry generation, the grain size distributions are approximated using either the lognormal or RRSB distribution. In addition, the equivalent thermal conductivity of the unresolved material k_{rest} is estimated from the effective medium theory. Employing the temperature-dependent thermal conductivities of the constituents, an overestimation of k_{eff} as compared to its experimental values, particularly at low to moderate temperatures, is found. Consequently, the thermal expansion of the coarse and the medium grains is considered and modelled by introducing an air gap that decreases at higher temperatures between the grains and the continuous phase. Accounting for this gap width as a function of temperature in the FVM code that is employed for solving the associated heat conduction problem, the numerical predictions are significantly improved and qualitatively represent the measured k_{eff} in the entire range from the room to the coking temperature.

Prospective investigation may treat thermal expansion using a more detailed model and examine its effect on the numerical predictions. The employed equivalent thermal conductivity k_{rest} of the unresolved constituents, which is an extremely important parameter for the numerical model⁸, could be determined from both fine-scale model with a resolution of less than 10 μm and measurement of k_{rest} for the separately produced fine-scaled material.

Acknowledgement

The authors would like to gratefully acknowledge the financial support from the German Research Foundation (DFG) under the grants TR 470/2–1 and TR 470/2–2 in the framework of the priority programme SPP 1418 “Refractories-Initiative to Reduce Emissions” (FIRE). The authors would like to thank Dr A. Mertke and Dr G. Schmidt of the Institute of Ceramic, Glass and Construction Materials, TU Bergakademie Freiberg, Germany, for preparing the refractory material R20 used in this investigation and the SEM analysis, respectively.

References

- Roungos, V., Aneziris, C.G.: Improved thermal shock performance of Al_2O_3 -C refractories due to nanoscaled additives, *Ceram. Int.*, **38**, 919–927, (2012).
- Roungos, V., Aneziris, C.G., Berek, H.: Novel Al_2O_3 -C refractories with less residual carbon due to nanoscaled additives for continuous steel casting applications, *Adv. Eng. Mater.*, **14**, 255–264, (2012).
- Stein, V., Aneziris, C.G.: Low-carbon carbon-bonded alumina refractories for functional components in steel technology, *J. Ceram. Sci. Tech.*, **5**, 115–123, (2014).
- Chesters, J.H.: Refractories for iron- and steelmaking. The Metals Society, London, 1974.
- Ruan, G.Z., Li, N.: Carbon pickup of interstitial free steel from Al_2O_3 -C refractories, *Ironmak Steelmak*, **31**, 342–344, (2004).
- Zhang, L., Thomas, B.G.: State of the art in evaluation and control of steel cleanliness, *ISIJ Int.*, **43**, 271–291, (2003).
- Zehmisch, R., Al-Zoubi, A., Ray, S., Trimis, D., Ballani, F., van den Boogaart, K.G.: Numerical determination of effective thermal conductivity of refractory materials, *Refractories Worldforum*, **4**, 181–186, (2012).
- Zehmisch, R., Demuth, C., Al-Zoubi, A., Mendes, M.A.A., Ballani, F., Ray, S., Trimis, D.: Numerical prediction of effective thermal conductivity of refractory materials: methodology and sensitivity analysis, *J. Ceram. Sci. Tech.*, **5**, 145–153, (2014).
- Wang, M., Pan, N.: Predictions of effective physical properties of complex multiphase materials, *Mater. Sci. Eng., R*, **63**, 1–30, (2008).
- Rosin, P., Rammler, E.: The laws governing the fineness of powdered coal, *J. Inst. Fuel*, **7**, 29–36, (1933).
- Rosin, P., Rammler, E., Sperling, K.: Grain size problems of coal dust and their significance for crushing, in German, *Berichte der Technisch-Wirtschaftlichen Sachverständigenausschüsse des Reichskohlenrats*, **C 52**, 25 pp., VDI-Verlag, Berlin, 1933.
- Bennett, J.G.: Broken coal, *J. Inst. Fuel*, **10**, 22–39, (1936).
- Petrasch, J., Schrader, B., Wyss, P., Steinfeld, A.: Tomography-based determination of the effective thermal conductivity of fluid-saturated reticulate porous ceramics, *J. Heat Transfer*, **130**, 032602 (10 pp.), (2008).
- Coquard, R., Baillis, D.: Numerical investigation of conductive heat transfer in high-porosity foams, *Acta Mater.*, **57**, 5466–5479, (2009).
- Mendes, M.A.A., Ray, S., Trimis, D.: A simple and efficient method for the evaluation of effective thermal conductivity of open-cell foam-like structures, *Int. J. Heat Mass Transf.*, **66**, 412–422, (2013).
- Lee, W.E., Zhang, S., Karakus, M.: Refractories: controlled microstructure composites for extreme environments, *J. Mater. Sci.*, **39**, 6675–6685, (2004).
- Werner, J., Aneziris, C.G., Dudczig, S.: Young’s modulus of elasticity of carbon-bonded alumina materials up to 1450 °C, *J. Am. Ceram. Soc.*, **96**, 2958–2965, (2013).
- Modest, M.F.: Radiative heat transfer. 3rd edition. Academic Press, New York, 2013.
- Mendes, M.A.A., Talukdar, P., Ray, S., Trimis, D.: Detailed and simplified models for evaluation of effective thermal conductivity of open-cell porous foams at high temperatures in presence of thermal radiation, *Int. J. Heat Mass Transf.*, **68**, 612–624, (2014).
- Mendes, M.A.A., Skibina, V., Talukdar, P., Wulf, R., Gross, U., Trimis, D., Ray, S.: Experimental validation of simplified conduction-radiation models for evaluation of effective thermal conductivity of open-cell metal foams at high temperatures, *Int. J. Heat Mass Transf.*, **78**, 112–120, (2014).
- Mertke, A., Aneziris, C.G.: The influence of nanoparticles and functional metallic additions on the thermal shock resistance of carbon bonded alumina refractories, *Ceram. Int.*, **41**, 1541–1552, (2015).
- Routschka, G. (Ed.): Pocket manual refractory materials: basics, structures, properties. 2nd edition. Vulkan-Verlag, Essen, 2004.
- Fruhstorfer, J., Aneziris, C.G.: The influence of the coarse fraction on the porosity of refractory castables, *J. Ceram. Sci. Tech.*, **5**, 155–165, (2014).
- Rahaman, M.N.: Ceramic processing. In: Kirk, R.E., Othmer, D.F. (Eds.): Kirk-Othmer encyclopedia of chemical technology, John Wiley & Sons, Inc., Hoboken, 1–98, 2014.
- Reed, J.S.: Introduction to the principles of ceramic processing, John Wiley & Sons, Inc., New York, pp. 188 ff., 1988.
- Stein, V.: Contribution to the characteristic improvement of carbon bonded doloma refractories by addition of functional ceramic materials, Ph.D. thesis, Technische Universität Bergakademie Freiberg, Freiburger Forschungshefte, A 905, (2011).
- Schwieger, K.-H.: Refractory materials (in German). In: Becker, G.W., Braun, D., Woebcken, W. (Eds.): Kunststoffhandbuch (Plastics manual), Vol.10 Duroplaste (Thermosetting plastics). Carl Hanser Verlag, München, 1096–1104, 1988.

- ²⁸ Irie, S., Rappolt, J.: Phenolic resin for refractories. In: Pilato, L.: Phenolic Resins: A Century of Progress. Springer-Verlag, Berlin, chapter 19, 503–515, 2010.
- ²⁹ Tomeczek, J., Suwak, R.: Thermal conductivity of carbon-containing refractories, *Ceram. Int.*, **28**, 601–607, (2002).
- ³⁰ Weibull, W.: A statistical distribution function of wide applicability, *J. Appl. Mech.*, **18**, 293–297, (1951).
- ³¹ Bernhardt, C.: Particle size analysis – classification and sedimentation methods. Powder Technology Series. Chapman & Hall, London, 1994.
- ³² Sommer, K.: 40 years of presentation particle size distributions – yet still incorrect?, *Part. Part. Syst. Charact.*, **18**, 22–25, (2001).
- ³³ Sties, M.: Mechanical process engineering – particle technology. 3rd, revised edition (in German). Springer, Berlin, 2009.
- ³⁴ Leva, J.L.: A fast normal random number generator, *ACM Trans. Math. Software*, **18**, 449–453, (1992).
- ³⁵ Press, W.H., Teukolsky, S.A., Vetterling, W.T., Flannery, B.P.: Numerical recipes: the art of scientific computing. 3rd edition. Cambridge University Press, Cambridge, 2007.
- ³⁶ He, D., Ekere, N.N., Cai, L.: Computer simulation of random packing of unequal particles, *Phys. Rev. E*, **60**, 7098–7104, (1999).
- ³⁷ Knuth, D.E.: Seminumerical algorithms. The art of computer programming, Vol. 2. 3rd edition. Addison-Wesley, Reading, MA, 1997.
- ³⁸ Goldstein, H., Poole, C.P., Safko, J.L.: Classical mechanics. 3rd edition. Addison-Wesley, San Francisco, 2002.
- ³⁹ Ballani, F., Daley, D.J., Stoyan, D.: Modelling the microstructure of concrete with spherical grains, *Comput. Mater. Sci.*, **35**, 399–407, (2006).
- ⁴⁰ Hashin, Z., Shtrikman, S.: A variational approach to the theory of the effective magnetic permeability of multiphase materials, *J. Appl. Phys.*, **33**, 3125–3131, (1962).
- ⁴¹ Kirkpatrick, S.: Percolation and conduction, *Rev. Mod. Phys.*, **45**, 574–588, (1973).
- ⁴² Jiang, F., Sousa, A.C.M.: Effective thermal conductivity of heterogeneous multi-component materials: an SPH implementation, *Heat Mass Transfer*, **43**, 479–491, (2007).
- ⁴³ Hestenes, M.R., Stiefel, E.: Methods of conjugate gradients for solving linear systems, *J. Res. Natl. Bur. Stand.*, **49**, 409–436, (1952).
- ⁴⁴ Demuth, C., Mendes, M.A.A., Ray, S., Trimis, D.: Performance of thermal lattice Boltzmann and finite volume methods for the solution of heat conduction equation in 2D and 3D composite media with inclined and curved interfaces, *Int. J. Heat Mass Transf.*, **77**, 979–994, (2014).
- ⁴⁵ Dos Santos, W.N., Taylor, R.: Effect of porosity on the thermal conductivity of alumina, *High Temp.-High Press.*, **25**, 89–98, (1993).
- ⁴⁶ Ho, C.Y., Powell, R.W., Liley, P.E.: Thermal conductivity of the elements: a comprehensive review, *J. Phys. Chem. Ref. Data, Suppl.*, **3**, 1–796, (1974).
- ⁴⁷ Span, R.: Properties of dry air. In: Stephan, P. (Ed.): VDI Heat Atlas. 2nd edition. Springer-Verlag, Berlin, Heidelberg, 172–191, 2010.
- ⁴⁸ Touloukian, Y.S., Kirby, R.K., Taylor, E.R., Lee, T.Y.R.: Thermal expansion, Nonmetallic Solids. Vol. 13 in Touloukian, Y.S., Ho, C.Y. (Eds.): Thermophysical properties of matter: The TPRC Data Series; a Comprehensive Compilation of Data. IFI/Plenum, New York, 1977.
- ⁴⁹ Fiquet, G., Richet, P., Montagnac, G.: High-temperature thermal expansion relationship of lime, periclase, corundum and spinel, *Phys. Chem. Miner.*, **27**, 103–111, (1999).
- ⁵⁰ Riley, D.P.: The thermal expansion of graphite: part II. Theoretical, *Proc. Phys. Soc. London*, **57**, 486–495, (1945).
- ⁵¹ Tsang, D.K.L., Marsden, B.J., Fok, S.L., Hall, G.: Graphite thermal expansion relationship for different temperature ranges, *Carbon*, **43**, 2902–2906, (2005).
- ⁵² Loretz, M., Maire, E., Baillis, D.: Analytical modelling of the radiative properties of metallic foams: contribution of X-ray tomography, *Adv. Eng. Mater.*, **10**, 352–360, (2008).
- ⁵³ Brewster, Q.: Volume scattering of radiation in packed beds of large, opaque spheres, *J. Heat Transf.*, **126**, 1048–1050, (2004).
- ⁵⁴ Palik, E.D. (Ed.): Handbook of optical constants of solids, Vol. II. Academic Press, San Diego, 1991.